IEEE Access
Multidisciplinary ⋮ Rapid Review ⋮ Open Access Journal

Received April 19, 2021, accepted May 18, 2021, date of publication May 26, 2021, date of current version June 8, 2021.

Digital Object Identifier 10.1109/ACCESS.2021.3083936

Extended Spectra-Based Grid Map Merging With Unilateral Observations for Multi-Robot SLAM

HEONCHEOL LEE[1], (Member, IEEE), AND SEUNGHWAN LEE[2], (Member, IEEE)
[1]Department of IT Convergence Engineering, School of Electronic Engineering, Kumoh National Institute of Technology, Gumi 39177, Republic of Korea
[2]School of Electronic Engineering, Kumoh National Institute of Technology, Gumi 39177, Republic of Korea

Corresponding author: Heoncheol Lee (hclee@kumoh.ac.kr)

This work was supported in part by the National Research Foundation of Korea (NRF) grant through the Korea Government (MSIT) under Grant 2019R1G1A1100597, and in part by the Theater Defense Research Center through Defense Acquisition Program Administration under Grant UD200043CD.

ABSTRACT This paper deals with the problem of grid map merging in multi-robot SLAM (simultaneous positioning and mapping) where the initial relative pose between robots is unknown. When robots encounter each other, it is easy to obtain a map transformation between robots for grid map merging if bilateral observation measurements are available between robots. However, since the bilateral observation measurements are obtained by encounters between robots, they may limit the availability of using multi-robot systems. To overcome the limitation, spectra-based map merging can be applied without any observation measurements between robots. However, it requires sufficient overlapping areas between indivisual maps of robots, which can also limit the availability of using multi-robot systems. In this paper, therefore, to overcome both limitations, an extension of spectra-based map merging using not bilateral but unilateral observation measurements. The proposed method was tested with datasets obtained from real experiments with mobile robots equipped with a sensor fusion system which can obtain unilateral observation measurements to other robots. Experimental results showed that the proposed map merging method works successfully without any bilateral observation measurements.

INDEX TERMS Spectra-based map merging, unilateral observations, multi-robot systems.

I. INTRODUCTION

Multi-robot systems (MRS) have gained a great popularity where they can simultaneously perform two or more tasks in a shorter time than a single robot system. One of the important considerations to implement the MRS is to provide accurate information on the surrounding environment such as a collective feature map and a collective grid map. Generally a collective grid map can provide the shapes and positions of structures and obstacles well. If the collective grid map is not given, each robot firstly needs to create a grid map of its surrounding environments [1] before it conducts its own mission. Then, a collective grid maps can be obtained by accurately merging the individual grid maps. From the merged grid map, robots can share the information about areas the robot has not navigated, and thus efficient path planning can be utilized in subsequent missions.

A. GRID MAP MERGING

The map merging problem can be easily solved if the relative position and orientation between robots are given from a global positioning system (GPS) or a motion capture system at the start or during operation. However, if they are not given, robots have to find a map transformation between them to build a collective map. If relative initial poses are known, the map transformation can be easily obtained since the robot poses can be represented in a common coordinate system at the start. However, even if they are unknown, a collective map should be obtained by map merging methods which can be divided into direct map merging methods and indirect map merging methods. Direct map merging methods is to find a map transformation by using observation measurements from an internal onboard sensor system or an external structural sensor system. Indirect map merging methods is to find a map transformation by autonomously finding and matching the overlapping areas between individual grid maps.

B. RELATED WORKS

The direct map merging method utilizes bilateral observation measurements and common visual objects. In bilateral observation-based map merging methods [2], [8], map merging is conducted by observing the relative distances and angles between the robots at a predetermined point (rendezvous) or by accident. However, predetermined or

The associate editor coordinating the review of this manuscript and approving it for publication was Tao Liu.

This work is licensed under a Creative Commons Attribution 4.0 License. For more information, see https://creativecommons.org/licenses/by/4.0/

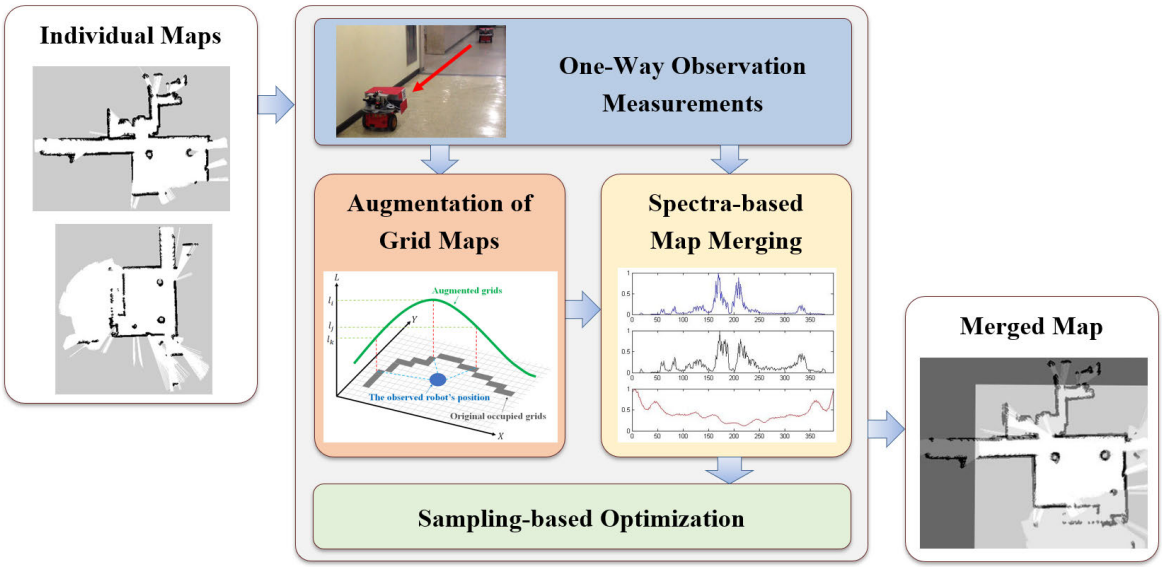

FIGURE 1. The overall structure of the proposed method. Unilateral observation measurements are used to augment grid maps and reduce the search space of the components of a map transformation matrix (MTM) for map merging. Then, the spectra-based map merging algorithm is conducted to estimate the MTM within the reduced search space. Finally, the more accurate MTM is obtained by the sampling-based optimization method within the more reduced search space with a margin vector caused by inevitable structural errors in the sensor fusion system.

accidental encounter conditions reduce the efficiency of the operation of the multi-robot system. In addition, since the accuracy of map merging depends on direct bilateral observation measurements, highly accurate sensors and data processing techniques are required, which increases the cost of configuring the multi-robot systems. In common object-based map merging methods [3], [9], map merging is conducted by recognizing common objects that are known to each other between robots and their relative locations and directions. However, since they need to predetermine the number, type and location of common objects, they are not practical in unknown environments.

The indirect map merging method utilizes an algorithm that matches the visual descriptors, geometric structures and mathematical features of individual maps. In the descriptor-based map merging methods [1], [10], [11], map merging is conducted by recognizing common objects that are known to each other between robots and their relative locations and directions. However, since it requires to extract the visual descriptor relatively high computational cost, it may burden real-time performance. Although several works have used visual features online, they still have the potential to become a bottleneck for real-time performance. In scan matching-based map merging methods [12], [13], map merging is conducted by finding and matching the overlapping areas using scan matching algorithms. However, since a sufficient amount of overlapping area is required, the efficiency of operation of a multi-robot system may be deteriorated. In the overlap-based map merging methods [5], [14], [17], map merging is conducted by finding and matching the overlapping areas using additional features extracted by mathematical transform methods such as Hough transformation [15] and Radon transformation [16]. TSD (truncated signed distances) grid-based map merging algorithm [17] has been developed to perform multi-agent TSD-SLAM. Their algorithm was tested in real rescue systems with smart helmets equipped with IMU (inertial measurement unit) and LIDAR (light detection and ranging) sensors. These indirect map merging techniques have used to overcome the practical constraint such as unknown or partially-known initial poses among robots. However, they generally have an inevitable problem, which is that there is a local minimum value in the search space in the matching algorithm.

C. OVERVIEW

Through the related works and our previous works [5], [6], we have learned that it is difficult to find an accurate MTM by solely using indirect map merging methods due to the inevitable problem of local minima. On the contrary, we have also learned that it is difficult to find an accurate MTM without indirect map merging methods due to the inevitable sensor errors and too large search spaces [4], [7]. Therefore, in this work, we have focused a combinational approach to use not only an indirect map merging method but also a direct map merging method to take their advantages. The core idea of this paper is to use a unilateral observation system as shown in Fig. 1 instead of a bilateral observation system to alleviate conditions in predetermined or accidental encounters that can reduce the efficiency of multi-robot system operation. In addition, the resulting ambiguity in the relative poses between robots is solved by the spectra-based map merging

algorithm within the search space reduced by the unilateral observation measurements. Finally, a sampling-based optimization algorithm is used to find the more accurate MTM within the more reduced search space with a margin vector caused by inevitable structural errors in the sensor fusion system. Consequently, the risk of local minima could be successfully avoided and the map merging could be accurately conducted.

The remainder of this paper is organized as follows. Section 2 describes the formulations of map merging in multi-robot systems including the definition of the map transformation matrix and the configuration of a general bilateral observation system. Section 3 presents the proposed method including the unilateral observation system, grid map augmentation, spectra-based map merging with the augmented grid maps, and sampling-based optimization. In Section 4, the evaluation results of the proposed method are described. Finally, Section 5 gives conclusions.

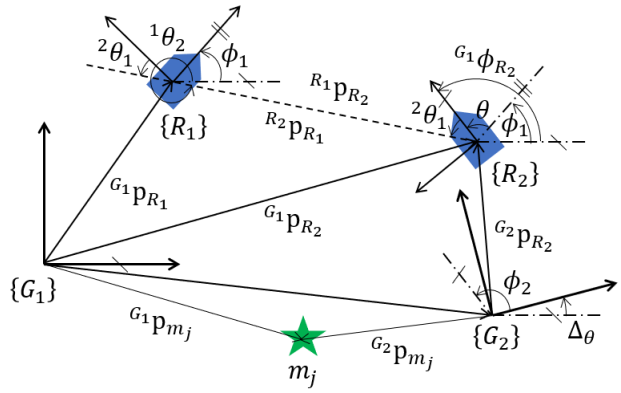

FIGURE 2. The geometry of a bilateral observation system when two robots encounter each other. The relative angle, θ, between the two robot frames $\{R_1\}$ and $\{R_2\}$ is represented as a function of the two orientation measurements $^1\theta_2$ and $^2\theta_1$. Based on θ, the rotation angle Δ_θ between two individual maps with the two global frames $\{G_1\}$ and $\{G_2\}$ can be estimated as a function of the two robot orientation angles ϕ_1 and ϕ_2. Finally, all the grids in $\mathbf{M}_1$ and $\mathbf{M}_2$ are commonly expressed with respect to $\{G_1\}$.

II. PROBLEM FORMULATION

A. MAP TRANSFORMATION MATRIX (MTM)

The map transformation between robots for map merging can be obtained in various ways as described in the previous section. In our previous works and related works, a two dimensional grid map $\mathbf{M}$ is assumed as a matrix with n_r rows and n_c columns for convenient implementation of map merging algorithms. In other words, a grid map can be regarded as a $n_r \times n_c$ binary image. Every grid contains map information on the location represented by the grid in the global coordinate system. Although the map merging problem can be regarded as an image matching problem, there is several differences. The most big difference is that individual maps produced from the same areas can be even different since the individual maps of different robots varies according to the robot trajectories.

For easy computation of map transformation, a dual form of $\mathbf{M}$is defined as a matrix with three rows and N_{occ} columns, which is denoted by $\mathbf{M}^d$. N_{occ} is the number of occupied grids in $\mathbf{M}$. The first and second rows of $\mathbf{M}^d$ represent x-coordinate and y-coordinate of the occupied grids, respectively. The last row of $\mathbf{M}^d$ is filled with 1 so that the computation with a map transformation matrix (MTM) is performed conveniently. Given two grid maps, $\mathbf{M}_1$ and $\mathbf{M}_2$, the MTM $\mathbf{T}$ which translates Δ_x in the direction of x-coordinate and Δ_y in the direction of y-coordinate, and rotates Δ_θ in a counter-clockwise is defined as follows:

$$\mathbf{T}(\Delta_x, \Delta_y, \Delta_\theta) = \begin{bmatrix} \cos\Delta_\theta & -\sin\Delta_\theta & \Delta_x \\ \sin\Delta_\theta & \cos\Delta_\theta & \Delta_y \\ 0 & 0 & 1 \end{bmatrix} \tag{1}$$

where $\mathbf{M}_2'^d = \mathbf{T}\mathbf{M}_2$. Here, $\mathbf{M}_2'^d$ is a new map rotated and translated from $\mathbf{M}_2^d$, which is represented in the same coordinate system with $\mathbf{M}_1$.

B. BILATERAL OBSERVATION SYSTEM

When the relative initial poses between robots are unknown, it is difficult to obtain the MTM at the start or during operation. If the individual maps overlap each other enough, various indirect map merging techniques can easily find the global minimum. However, since it is not guaranteed to overlap each other enough in a real environment, the indirect map merging technique always risks a local minimum. Therefore, the map merging needs to be conducted by combining more than two methods in order to utilize the respective advantages of the direct map merging method and the indirect map merging method. In this work, we focused on the advantage of the direct map merging method to reduce the search space in the indirect map merging method. Among direct map merging methods, we have excluded the common object-based map merging methods because they requires many predetermined factors such as the number, type and location of common objects, they are not being considered.

As a direct map merging method, bilateral observation-based map merging techniques require also the inevitable condition on predetermined or accidental encounters degenerates the efficiency of operating multi-robot systems. Figure 2 describes the general geometric coordinate system of a two-robot system which uses bilateral observation-based map merging methods [2], [8]. Note that the inefficiecy of using bilateral observation measurements is caused by the closely correlated geometric parameters at the encounters between robots. Let the robot 1 and robot 2 denote as R_1 and R_2, respectively. Then, two robots' frames can be denoted by $\{R_1\}$ and $\{R_2\}$. $^{G_1}\mathbf{P}_{R_i}$ is the position of the R_i's frame in the global frame $\{G_i\}$, where $i = 1,2$. The position of the R_j's frame in the R_i's frame is denoted by $^{R_i}\mathbf{P}_{R_j}$, where $j = 1,2$. ϕ_i is the orientation of R_i in the global frame $\{G_i\}$. $^i\theta_j$ is the angle between the R_i's orientation and the position vector of R_j in

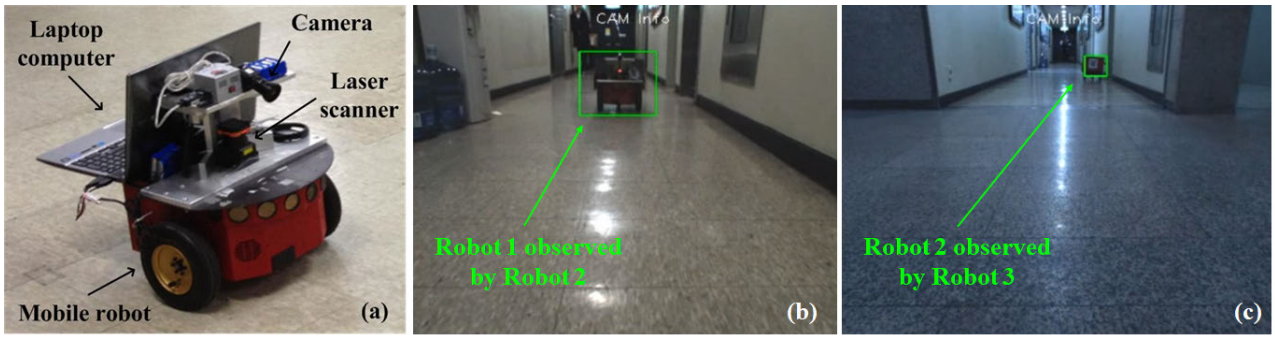

FIGURE 3. Unilateral observation system configuration for cooperative robot mapping. (a) Each robot in multi-robot systems has a sensor fusion system with a laser scanner and a monocular camera to recognize other robots. (b) Robot 1 was observed by Robot 2, and the unilateral measurement from Robot 2 to Robot 1 was obtained by sensor fusion. (c) Robot 2 was observed by Robot 3, and the unilateral measurement from Robot 3 to Robot 2 was obtained by sensor fusion. The map merging process is conducted based on not bilateral observation measurements between robots but these unilateral observation measurements.

the R_i's frame. θ is the angle between the R_i's orientation and the R_j's orientation.

The derivation processes of the formulas to calculate the rotation angle and translation amounts are described in [2], [8]. Consequently, the rotation angle Δ_θ which is one of the components of the MTM can be respectively calculated as follows:

$$\Delta_\theta = \phi_1 - \phi_2 + \theta \tag{2}$$

where $\theta =^1 \theta_2 -^2 \theta_1 - \pi$. The translation amounts Δ_x and Δ_y of $\{G_2\}$ in $\{G_1\}$ can be respectively calculated as follows:

$$\begin{bmatrix} \Delta_x \\ \Delta_y \end{bmatrix} =^{G_1} \mathbf{P}_{G_2} =^{G_1} \mathbf{P}_{R_1} + \mathbf{C}(\phi_1)^{R_1}\mathbf{P}_{R_2} - \mathbf{C}(\Delta_\theta)^{G_2}\mathbf{P}_{R_2} \tag{3}$$

where $\mathbf{C}(\phi)$ is the rotation matrix with a rotation angle ϕ. Because geometric parameters are closely correlated, the performance of map merging methods can be degraded if only one is inaccurate due to sensor error or missing due to stringent conditions of the encounter. Therefore, this delicate but fragile technique needs to be extended in the context of robustness with a different observation system and an indirect map merging method. Therefore, this paper proposes an extension of spectra-based map merging with unilateral observation measurements instead of bilateral observation measurements.

III. PROPOSED METHOD

The proposed method is an extension of the spectra-based map merging (SMM) which uses unilateral observation measurements to improve the availability of multi-robot systems while maintaining the accuracy of map merging. The proposed method consists of four sequential parts as shown in Fig. 1. Firstly, when a robot R_i perceives another robot R_j visually, R_i estimates the relative position of R_j in the R_i's coordinate system by fusing the visual and range data, regardless of the corresponding perception from R_j. Then, the individual grid maps are augmented using the unilateral observation measurements to probabilistically reflect the perceived relative robot positions. Next, a MTM between R_i and R_j is obtained by the SMM within the reduced search space by the unilateral observation measurements. Finally, the more accurate MTM between R_i and R_j is obtained by a sampling-based optimization method within the more reduced search space with a margin vector caused by inevitable structural errors in the sensor fusion system.

A. UNILATERAL OBSERVATION SYSTEM

Each robot in the multi-robot system is equipped with a vision sensor, a laser scanner and a laptop computer as shown in Fig. 3(a). The detection of the robot was performed by a support vector machine-based classification method with a histogram of oriented gradient (HoG) features. Each robot's sides and back are surrounded by a paper board with predetermined tags attached to it for easy detection by visual sensors. The examples of the unilateral observation system-based detection are shown in Fig. 3(b) and Fig. 3(c), which shows that the front and back sides of a robot could be successfully detected. Once R_j is detected, the relative angle to R_j in the frame of R_i is roughly provided by counting the pixel distance from the center of the image. Then, the relative angle and distance from R_i to R_j are updated by selecting the mean of the salient points on the direction of the roughly provided relative angle in the laser scanner data. This process was conducted with an assumption that the detected robot was located in uncluttered areas. The assumption may be relaxed by combining more complex image processing to detect another robot more accurately and direct depth information with a stereo camera. Finally, the relative position ${}^{R_i}\mathbf{P}_{R_j}$ is obtained by converting the relative angle and distance into the Cartesian coordinate system $\{R_i\}$.

In the unilateral observation systems, two problems are addressed to apply the equations (2) and (3) to accurate map merging. The first problem of the unilateral observation system is the absence of ${}^2\theta_1$ in Fig. 2, which is critical to calculate not only the relative rotation angle Δ_θ but also the translation amounts Δ_x and Δ_y. The second problem of the unilateral observation system is the accuracy of ${}^{R_1}\mathbf{P}_{R_2}$. Because we did

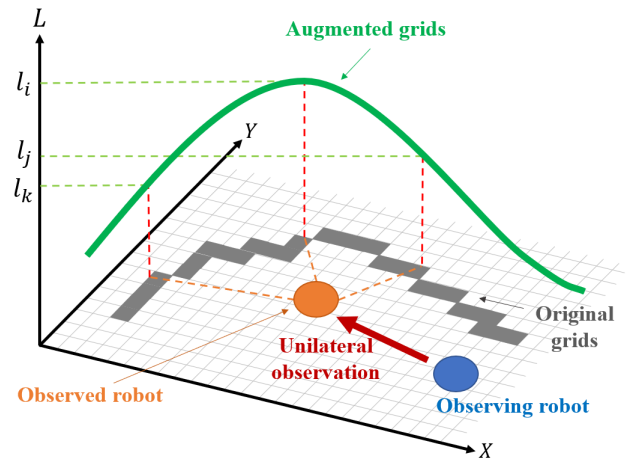

FIGURE 4. The concept of augmenting the occupancy grids. X-axis and Y-axis indicate Cartesian coordinates, and L-axis indicates the augmentation level. Each original occupied grid is augmented along to the multivariate Gaussian distribution with the mean and covariance of the robot position by a unilateral observation measurement. l_i, l_j, and l_k are the augmented levels, and the closer grid to the robot position gets the more augmented level. This augmentation is applied to both grid maps.

not use any rendezvous points, R_1 observes accidently R_2, which means that R_2 moves to its own goal and does not wait until R_1 obtains more accurate range measurements. Thus, ${}^{R_1}\mathbf{P}_{R_2}$ may be inaccurate. In bilateral observation systems, the errors in ${}^{R_1}\mathbf{P}_{R_2}$ can be compensated by ${}^{R_2}\mathbf{P}_{R_1}$. However, in the unilateral observation systems, the relative distance measurements depends on only ${}^{R_1}\mathbf{P}_{R_2}$.

B. AUGMENTATION OF GRID MAPS

To solve the two problems of the unilateral observation system, the occupied grid is augmented so that the area around the observed robot can be distinguished from other areas. The following is one stackup notifying that the observed robot, R_2, is currently being observed by R_1 even though it cannot observe R_1. The concept of occupying grid expansion can be seen in Fig. 4. The occupied grid of R_1 is augmented with the mean and covariance of the relative R_2 positions by unilateral observational measurements. The occupied grid of R_2 is augmented with the mean and covariance of its own position when notified that it is being observed by another robot.

The original grid maps of R_1 and R_2 at the frame 615 are respectively shown in Fig. 5, and the original grid maps of R_2 and R_3 at the frame 513 are respectively shown in Fig. 7. The augmentation value at the location of the n-th occupied grid, $\mathbf{m}_{i,n} = [x_{i,n}, y_{i,n}]$, in $\mathbf{M}_i$ is determined along to the multivariate Gaussian distribution with the mean $\widehat{\mathbf{x}}_i$ and covariance Σ_{aug} of the robot position estimated by a unilateral observation measurement as follows:

$$Aug(\mathbf{m}_{i,n}) = \frac{I_{aug}}{2\pi|\Sigma_{aug}|^{1/2}} \times \exp\left(-\frac{1}{2}(\mathbf{m}_{i,n} - \widehat{\mathbf{x}}_i)^T \Sigma_{aug}^{-1}(\mathbf{m}_{i,n} - \widehat{\mathbf{x}}_i)\right) \quad (4)$$

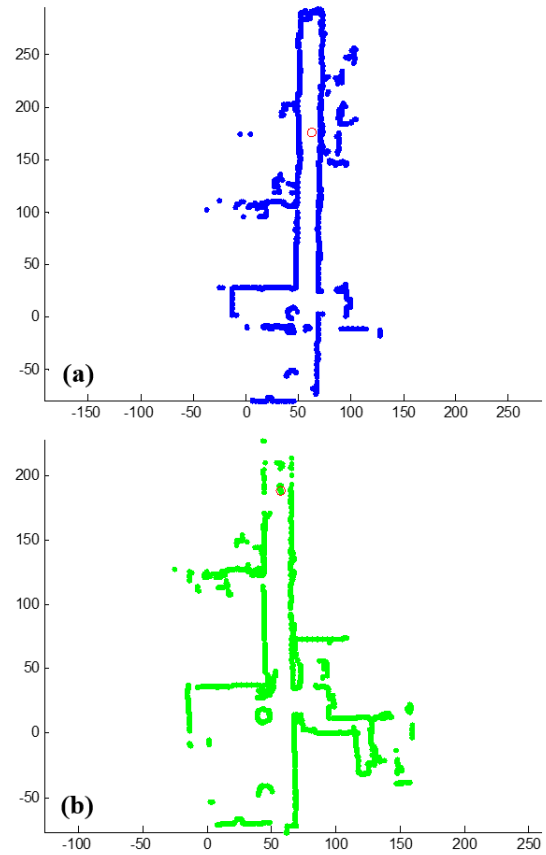

FIGURE 5. Original grid maps of R_1 and R_2 at the frame 615. The occupied grids in $\mathbf{M}_1$ and $\mathbf{M}_2$ are represented by blue and green colors, respectively. The red circles in each map are $\widehat{\mathbf{x}}_1$ and $\widehat{\mathbf{x}}_2$ for the augmentation, respectively. (a) R_1's dual grid map. (b) R_2's deal grid map.

where I_{aug} is the augmentation intensity, which is empirically determined. Then, the augmented map $\mathbf{M}_i^a$ for the locations $[x, y] \in \mathbf{M}_i$ is defined as follows:

$$\mathbf{M}_i^a(x, y) = \begin{cases} Aug([x, y]), & \text{if } \mathbf{M}_i(x, y) \text{ is occupied} \\ 0, & \text{otherwise} \end{cases} \quad (5)$$

In Fig. 5 and Fig. 7, the red circles in each map are $\widehat{\mathbf{x}}_i$ for the grid map augmentation. $\widehat{\mathbf{x}}_i$ in the observed robot map is identical to its own position, and $\widehat{\mathbf{x}}_i$ in the observing robot map can be obtained by the vector sum of its own position and the unilateral observation measurement. Therefore, $\widehat{\mathbf{x}}_i$ in both maps of the observed robot and observing robot indicates a similar position, which means that the augmentation patterns are also similar. This similarity is helpful for matching grid maps because it can reduce the search space of a MTM. The visualization of the augmented grid maps is shown in Fig. 6 and Fig. 8, which shows that the grids around $\widehat{\mathbf{x}}_i$ were more augmented.

C. SPECTRA-BASED MAP MERGING WITH UNILATERAL OBSERVATION

The spectra-based map merging (SMM) [14] is an approach to utilizing the spectral information to solve the problem of

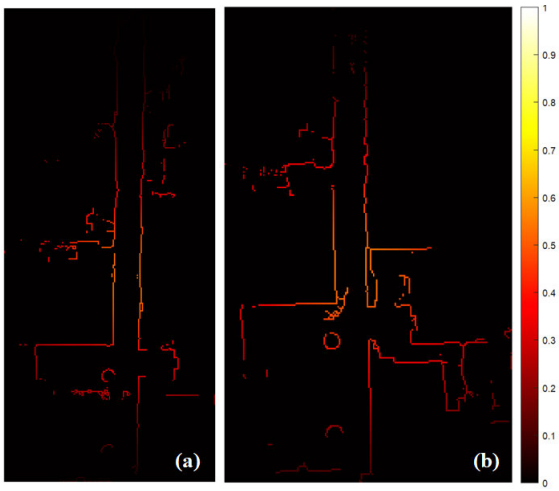

FIGURE 6. Augmented grid maps of R_1 and R_2 at the frame 615. The dual grid maps are augmented along to the multivariate Gaussian distribution by a unilateral observation measurement. (a) R_1's augmented grid map. (b) R_2's augmented grid map.

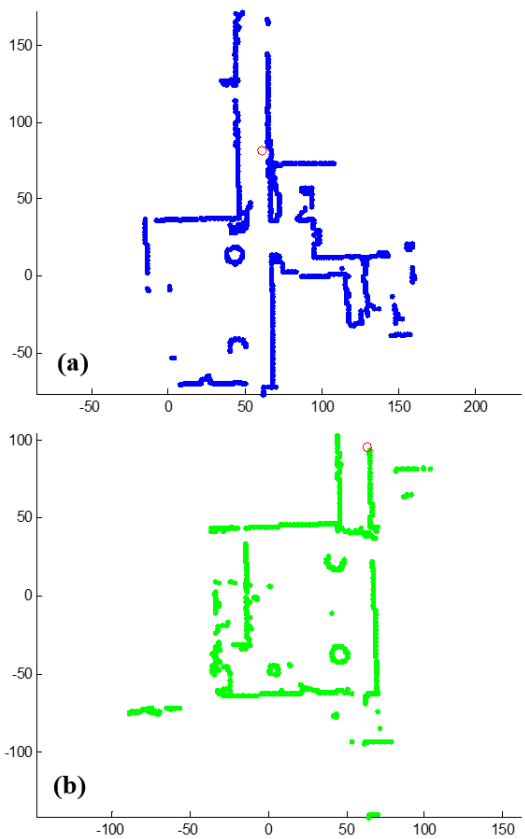

FIGURE 7. Original grid maps of R_2 and R_3 at the frame 513. The occupancy grid maps are represented by dual grid maps for easy computation of map transformation. The occupied grids in $\mathbf{M}_2$ and $\mathbf{M}_3$ are represented by blue and green colors, respectively. (a) R_2's dual grid map. (b) R_3's dual grid map.

map merging. The key idea of the SMM is to consider the map merging problem as the binary image matching problem. Firstly, the rotation angle between maps, Δ_θ, is estimated

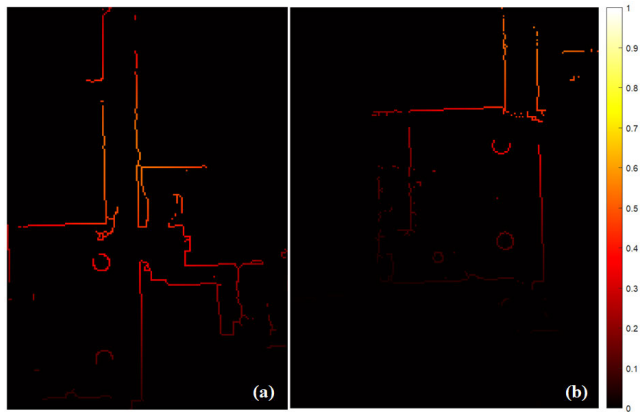

FIGURE 8. Augmented grid maps of R_2 and R_3 at the frame 513. The dual grid maps are augmented along to the multivariate Gaussian distribution by a unilateral observation measurement. (a) R_2's augmented grid map. (b) R_3's augmented grid map.

using the Hough spectrum [15] which is generated from the Hough transform, $x\cos\theta + y\sin\theta = \rho$, where θ is the angle between x-axis and the normal from the line to the origin, and ρ is the distance between the line and the origin. Then, x and y displacements, Δ_x and Δ_y, are estimated using X-spectrum and Y-spectrum, respectively.

Differently from the original SMM, in this work, the search space for the amount of transformation can be greatly reduced from $[a_1, a_2]$ and $[b_1, b_2]$ to $[\Delta_{x,min} - \sigma, \Delta_{x,max} + \sigma]$ and $[\Delta_{y,min} - \sigma, \Delta_{y,max} + \sigma]$ by unilateral observation measurements. In the equation (3), even though Δ_θ is uknown due to the absence of ${}^2\theta_1$, the minimum and the maximum results of applying the rotation matrix with Δ_θ can be calculated using the bounds of trigonometric functions as follows:

$$-\|{}^{G_2}\mathbf{P}_{R_2}\| \leq \mathbf{C}(\Delta_\theta){}^{G_2}\mathbf{P}_{R_2} \leq \|{}^{G_2}\mathbf{P}_{R_2}\| \tag{6}$$

where $\|\cdot\|$ represents the absolute-value of a vector.

Then, the minimum and the maximum results of the translational amounts Δ_x and Δ_y can be estimated respectively as follows:

$$\begin{bmatrix} \Delta_{x,min} \\ \Delta_{y,min} \end{bmatrix} = {}^{G_1}\mathbf{P}_{R_1} + \mathbf{C}(\phi_1){}^{R_1}\mathbf{P}_{R_2} - \|{}^{G_2}\mathbf{P}_{R_2}\| \tag{7}$$

$$\begin{bmatrix} \Delta_{x,max} \\ \Delta_{y,max} \end{bmatrix} = {}^{G_1}\mathbf{P}_{R_1} + \mathbf{C}(\phi_1){}^{R_1}\mathbf{P}_{R_2} + \|{}^{G_2}\mathbf{P}_{R_2}\| \tag{8}$$

Therefore, the reduced search space for Δ_x and Δ_y is respectively determined with the consideration of the errors in the unilateral observation measurements as follows:

$$\Delta_{x,min} - \sigma \leq \Delta_x \leq \Delta_{x,max} + \sigma \tag{9}$$

$$\Delta_{y,min} - \sigma \leq \Delta_y \leq \Delta_{y,max} + \sigma \tag{10}$$

where σ is a margin value reflecting the range error in the laser scanner. And the search space for Δ_θ is maintained as $-\pi \leq \Delta_\theta \leq \pi$ because the rotation angle Δ_θ cannot be obtained without ${}^2\theta_1$.

Let $\mathbf{M}$ and $\mathbf{M}_H$ be an augmented grid map and the result of Hough transform which is a matrix with n_ρ rows

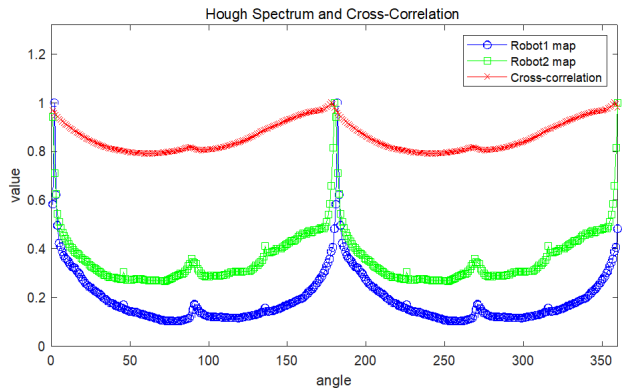

FIGURE 9. The Hough spectra and cross-correlation of the two individual augmented grid maps. The rotation angle between two individual maps is estimated by taking the angle corresponding to the maximum of the cross-correlation.

and n_θ columns, respectively. Its associated Hough spectrum for $1 \leq j \leq n_\theta$ is defined as the following unidimensional signal:

$$\mathbf{HS}_{\mathbf{M}}(j) = \sum_{i=1}^{n_\rho} \mathbf{M}_H(i,j)^2 \tag{11}$$

The signal has sampling period with $2\pi/n_\theta$ and indicates how frequently lines are detected along θ. Given Hough spectra, $\mathbf{HS}_{\mathbf{M}_1}$ and $\mathbf{HS}_{\mathbf{M}_2}$, circular cross correlation is computed to determine similarities along θ as follows:

$$\mathbf{CC}_{M_1\ M_2}(k) = \sum_{i=1}^{n_\theta} \mathbf{HS}_{\mathbf{M}_1}(i)\mathbf{HS}_{\mathbf{M}_2}(i+k) \tag{12}$$

The Hough spectra and cross-correlation of the two individual augmented grid maps are shown in Fig. 9. The SMM can estimate the rotation angle between two individual maps by taking the angle corresponding to the maximum of the cross-correlation: $\Delta_\theta = \arg\max_k \mathbf{CC}_{\mathbf{M}_1\mathbf{M}_2}(k)$. The search space for the rotation is as follows: $1 \leq k \leq n_\theta$ which is same as the original SMM.

If an augmented grid map $\mathbf{M}$ is considered as a binary image with r rows and c columns, X-spectrum for $1 \leq j \leq c$ and Y-spectrum for $1 \leq i \leq r$ are respectively defined as the following signals:

$$\mathbf{XS}_{\mathbf{M}}(j) = \sum_{i=1}^{r} \mathbf{M}(i,j) \tag{13}$$

$$\mathbf{YS}_{\mathbf{M}}(i) = \sum_{j=1}^{c} \mathbf{M}(i,j) \tag{14}$$

Given the optimal rotation, Δ_θ, we can obtain $\widetilde{\mathbf{M}}_2 = \mathbf{T}(0,0,\Delta_\theta)\mathbf{M}_2$. Similarly with $\mathbf{CC}_{\mathbf{M}_1\mathbf{M}_2}$, circular cross correlations are respectively computed to determine X and Y displacements as follows:

$$\mathbf{CX}_{\mathbf{M}_1\widetilde{\mathbf{M}}_2}(\tau) = \sum_{j=-\infty}^{+\infty} \mathbf{XS}_{\mathbf{M}_1}(j+\tau)\mathbf{XS}_{\mathbf{M}_2^\theta}(j) \tag{15}$$

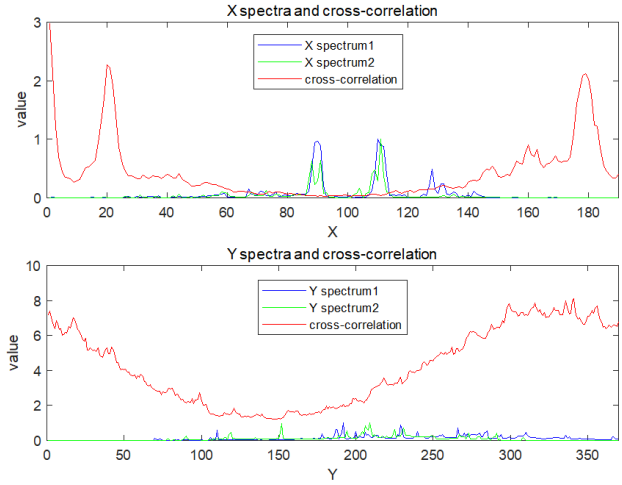

FIGURE 10. The X and Y spectra and cross-correlation of two augmented grid maps. The best X and Y translations between them are estimated by taking the amounts corresponding to the maximum of cross-correlations within the reduced search space by unilateral observation measurements.

$$\mathbf{CY}_{\mathbf{M}_1\widetilde{\mathbf{M}}_2}(\nu) = \sum_{i=-\infty}^{+\infty} \mathbf{YS}_{\mathbf{M}_1}(i+\nu)\mathbf{YS}_{\mathbf{M}_2^\theta}(i) \tag{16}$$

The X and Y spectra and cross-correlation of the two individual augmented grid maps are shown in Fig. 10. The SMM can estimate the X and Y translation amounts between two individual maps by taking the amounts corresponding to the maximum of the cross-correlations: $\Delta_x = \arg\max_\tau \mathbf{CX}_{\mathbf{M}_1\widetilde{\mathbf{M}}_2}(\tau)$, and $\Delta_y = \arg\max_\nu \mathbf{CY}_{\mathbf{M}_1\widetilde{\mathbf{M}}_2}(\nu)$. The search space for translations is as follows: $\Delta_{x,min} - \sigma \leq \tau \leq \Delta_{x,max} + \sigma$ and $\Delta_{y,min} - \sigma \leq \nu \leq \Delta_{y,max} + \sigma$. Differently from the original SMM, since the search space was reduced by the unilateral observation measurements, the risk of local minima was reduced. However, the map merging result by the SMM may be inaccurate due to the lack of overlapping areas between the spectral information of augmented grid maps. So, the MTM used for map merging needs to be optimized. In the context of optimization, the search space is significantly reduced by the result of the SMM where Δ_θ, Δ_x and Δ_y as shown in Fig. 11.

D. SAMPLING-BASED OPTIMIZATION

Since the SMM can find the MTM solely, one may not need more methods. However, the MTM obtained by the SMM may be inaccurate due to the inaccuracy of the individual maps caused by inevitable errors in sensors and the performance limitations of the matching algorithm. Therefore, it is necessary to apply an optimization method to obtain a more precise MTM. The objective function between two individual augmented grid maps $\mathbf{M}_1^{aug}$ and $\mathbf{M}_2^{aug}$ for a candidate MTM $\mathbf{t}_c$ is as follows:

$$\Gamma(\mathbf{M}_1^{aug}, \mathbf{M}_2^{aug}, \mathbf{t}_c) = \sum_{x=x_{min}}^{x_{max}} \sum_{y=y_{min}}^{y_{max}} \mathbf{M}_1^{aug}(x,y) \cdot \left[\mathbf{T}(\mathbf{t}_c)\mathbf{M}_2^{aug}(x,y)\right] \tag{17}$$

where x_{min} and x_{max} are the minimum and maximum of the allowable x-coordinate of $\mathbf{M}_1^{aug}$ and $\mathbf{M}_2^{aug}$. y_{min} and y_{max} are the minimum and maximum of the allowable y-coordinate of $\mathbf{M}_1^{aug}$ and $\mathbf{M}_2^{aug}$. Because this objective function is nonlinear, it is difficult to apply the conventional optimization method which provides a closed form for the optimal configuration to the optimization problem. Instead, sampling-based optimization methods can be applied to the optimization problem. However, they needs to be simple as much as possible to reduce the overall amount of computation required for map merging. In this paper, two sampling-based optimization methods are considered such as MCO (Monte-Carlo Optimization) [18] and PSO (Particle Swarm Optimization) [19]. Generally, the MCO and PSO require much computation time due to the iterative property, which becomes worse if the search space is wide. However, since the space space was significantly reduced by the results of the SMM with the unilateral observation measurements, the number of iterations required for convergence is quite reduced, which means that the computation time was significantly reduced.

1) MONTE-CARLO OPTIMIZATION

The MCO [18] is one of the sampling-based optimization algorithms that rely on repeated random sampling to obtain an optimal configuration in a given search space. The MCO has been widely used in a variety of scientific and engineering fields despite its large computational load. This is because it is simple to implement and shows good performance despite its complex and nonlinear constraints and its objective function. The processes of the MCO are as follows. First, the whole given search space is initialized, and the process of sampling the candidate configurations for the MTM is conducted around the MTM obtained by the SMM. Next, the range constraints for the sampled configuration are updated with considering the different sizes of maps. Then, the objective value matrix is iteratively updated based on the objective function for every sampled configuration. Finally, if the MCO reaches the predetermined number of samples, the configuration indicating the maximum in the objective value matrix is selected as the optimal configuration.

In the proposed method, the search space for the amount of transformation can be greatly reduced by the SMM with unilateral observation measurements as shown in the Fig. 11. The reduced search space for Δ_θ, Δ_x and Δ_y is respectively determined with the consideration of the errors in the unilateral observation measurements as follows:

$$\Delta_\theta - \sigma_\theta \leq \Delta_x \leq \Delta_\theta + \sigma_\theta \tag{18}$$

$$\Delta_x - \sigma_x \leq \Delta_x \leq \Delta_x + \sigma_x \tag{19}$$

$$\Delta_y - \sigma_y \leq \Delta_y \leq \Delta_y + \sigma_y \tag{20}$$

where $\Delta_\theta, \Delta_x and \Delta_y$ are the components of the MTM obtained by the SMM. $\sigma_\theta, \sigma_x and \sigma_y$ are margin values reflecting the orientation and range errors in the laser scanner, which depends on the quality of scan data. Even though the search space was significantly reduced by the SMM with the unilateral observation measurements as shown in Fig. 11, other sampling-based optimization methods such as PSO had to be considered in order to reduce the computation time as much as possible.

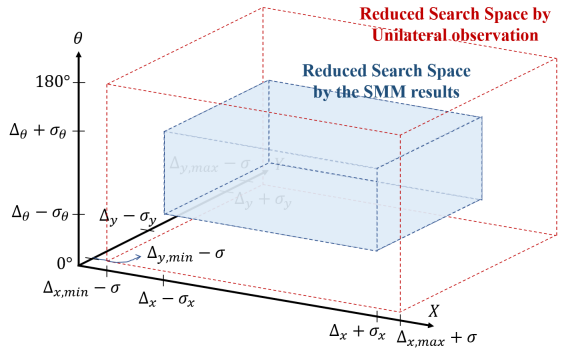

FIGURE 11. Reduced search space by the SMM results for the sampling-based optimization. The original search space where [0°180°], $[\Delta_{x,min} - \sigma, \Delta_{x,max} + \sigma]$ and $[\Delta_{y,min} - \sigma, \Delta_{y,max} + \sigma]$ was reduced as $[\Delta_\theta - \sigma_\theta, \Delta_\theta + \sigma_\theta]$, $[\Delta_x - \sigma_x, \Delta_x + \sigma_x]$ and $[\Delta_y - \sigma_y, \Delta_y + \sigma_y]$. The reduction was caused by the SMM result where Δ_θ, Δ_x and Δ_y.

2) PARTICLE SWARM OPTIMIZATION

PSO [19] is a sampling-based optimization algorithm based on cluster intelligence that solves an optimization problem by repeatedly moving particles representing a candidate solution to find an optimal solution for a given quality measurement. PSO has been widely used in various engineering fields because it can be implemented simply and has excellent performance even though the constraints and corresponding target functions are complex and nonlinear. The principle of particle movement in PSO is as follows. First, each particle is attracted by its target. Second, each particle has a memory of its own history. Third, all particles share velocity and position. Finally, each particle converges to the object as the iteration progresses. Based on these four principles, the particle cluster can find the optimal solution at the end of the iteration. The target function for map matching is nonlinear, so PSO can be a good solution for map merging. Besides, since the objective function is calculated with the augmented grid maps $\mathbf{M}_1^{aug}$ and $\mathbf{M}_2^{aug}$, it is expected to be converged faster. Moreover, since the search space for the amount of transformation was greatly reduced by the SMM with unilateral observation measurements as shown in the Fig. 11, the computation time for convergence was also significantly reduced. The reduced search space for the PSO was identical to that for the MCO in the previous subsection.

For every iteration with N_p particles, the velocity $\mathbf{v}_j(t)$ and position $\mathbf{p}_j(t)$ of each particle are respectively updated as follows:

$$\mathbf{v}_j(t+1) = \omega\left[\mathbf{v}_j(t) + \kappa\tau(\mathbf{p}_{sb} - \mathbf{p}_j(t)) + \kappa\tau(\mathbf{p}_{j,pb} - \mathbf{p}_j(t))\right] \tag{21}$$

$$\mathbf{p}_j(t+1) = \mathbf{p}_j(t) + \mathbf{v}_j(t+1) \tag{22}$$

where $\mathbf{p}_j(t) = [p_{j,x}, p_{j,y}, p_{j,\theta}]$ where $j = 1, \cdots, N_p$. $\omega < 1$ is a constriction factor which acts like friction, and $\kappa \sim [0, 1]$ is a random vector with uniform distribution, and $\tau \simeq 2$ is a control factor for relative attraction to $\mathbf{p}_{sb}$ and $\mathbf{p}_{j,pb}$. The personal best position $\mathbf{p}_{j,pb}$ indicates the best position of $\mathbf{p}_j$ so far with the maximum similarity between $\mathbf{M}_1^{aug}$ and $\mathbf{M}_2^{aug}$. The swarm best position $\mathbf{p}_{sb}$ indicates the position of the best particle throughout the whole particles and iterations. The objective function between $\mathbf{M}_1^{aug}$ and $\mathbf{M}_2^{aug}$ to measure the quality of each particle for map merging is defined in the equation (17). After the PSO is converged, the MTM $\mathbf{T}$ is determined as $\mathbf{T} = \mathbf{p}_{sb}$ at the final iteration.

IV. EXPERIMENTS

A. OVERALL RESULTS

To test and evaluate the proposed method, experiments using three robots were performed in an indoor environment. Each robot is equipped with a camera, laser scanner, and laptop computer as shown. 3(a). Each robot produced its own individual map in its own coordinate system using the previous SLAM (simultaneous localization and mapping) framework [2]. When the robot accidentally observes another robot, as shown in Fig. 3(b) and Fig. 3(c), the proposed method is performed using the unilateral observation measurements, the SMM and a sampling-based optimization method in order to obtain individual augmented grid maps and merge them as shown. 12. The augmentation levels were normalized. As expected, the grids around encounter positions between robots were highly augmented along the multivariate Gaussian distribution with the equation (4) and (5), which was useful to acquire an accurate MTM.

B. EVALUATION RESULTS

A performance index to measure how the individual grid maps are well aligned was defined to evaluate the accuracy in the merged grid map as follows [7]:

$$\Gamma(\mathbf{M}_1, \mathbf{M}_2^{tr}) = \frac{agr(\mathbf{M}_1, \mathbf{M}_2^{tr})}{N_{overlap}}. \tag{23}$$

where $agr(\cdot)$ is the number of the agreed grids in $\mathbf{M}_1$ and $\mathbf{M}_2^{tr}$ which is the transformed $\mathbf{M}_2$ by $\mathbf{T}$. $N_{overlap}$ is the number of grids in the real overlapping areas, which was acquired offline.

The accuracy of the proposed method may be affected by the intensity I_a and the covariance Σ_a which are the augmentation parameters. Therefore, the performance index according to the intensity I_a and the covariance Σ_a were investigated, while the number of particles for the PSO was fixed at 200 as shown in Fig. 13. While I_a did not affect the performance index, Σ_a had a significant influence on the performance index. Therefore, Σ_a has to be adjusted with considering the environments. In our experiments, Σ_a needed to be selected by more than 105 for merging $\mathbf{M}_1$ and $\mathbf{M}_2$ and 74 for merging $\mathbf{M}_2$ and $\mathbf{M}_3$, respectively.

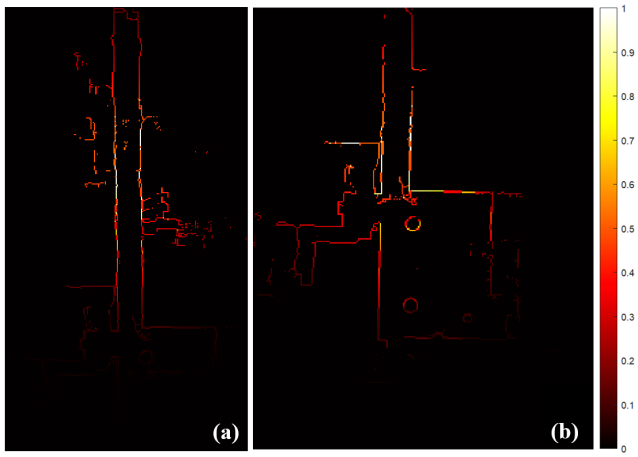

FIGURE 12. Merged augmented map. The two individual augmented grid maps were successfully merged with respect to a common coordinate system. The grids around encounter positions between robots were highly augmented, which was useful to acquire an accurate MTM. (a) Map merging result of $\mathbf{M}_1^{aug}$ and $\mathbf{M}_2^{aug}$ (b) Map merging result of $\mathbf{M}_2^{aug}$ and $\mathbf{M}_3^{aug}$.

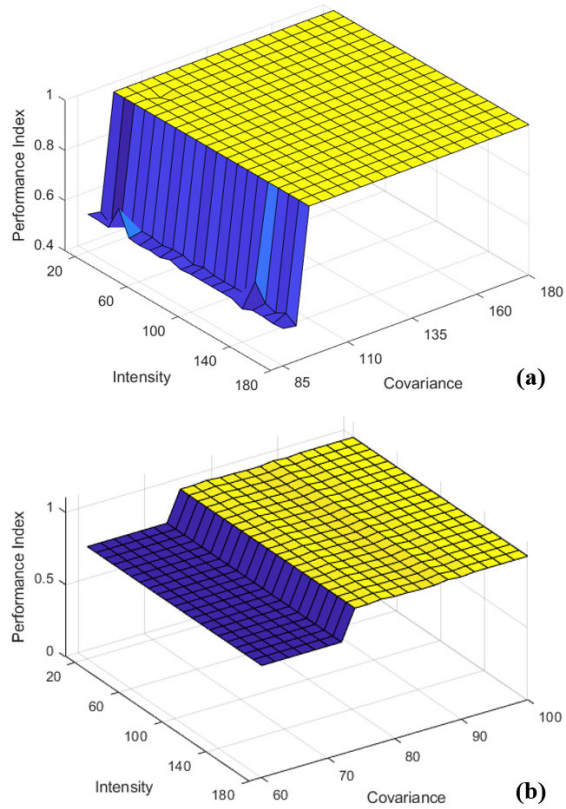

FIGURE 13. Performance indices according to the intensity and covariance for the augmentation. The performance index did not depend on the intensity but was affected by the covariance. (a) The case of merging $\mathbf{M}_1$ and $\mathbf{M}_2$ (b) The case of merging $\mathbf{M}_2$ and $\mathbf{M}_3$.

Because the proposed method utilizes the PSO as a sampling-based optimization method, the performance index and calculation time may be affected by the number of samples in the PSO. Therefore, the performance index and

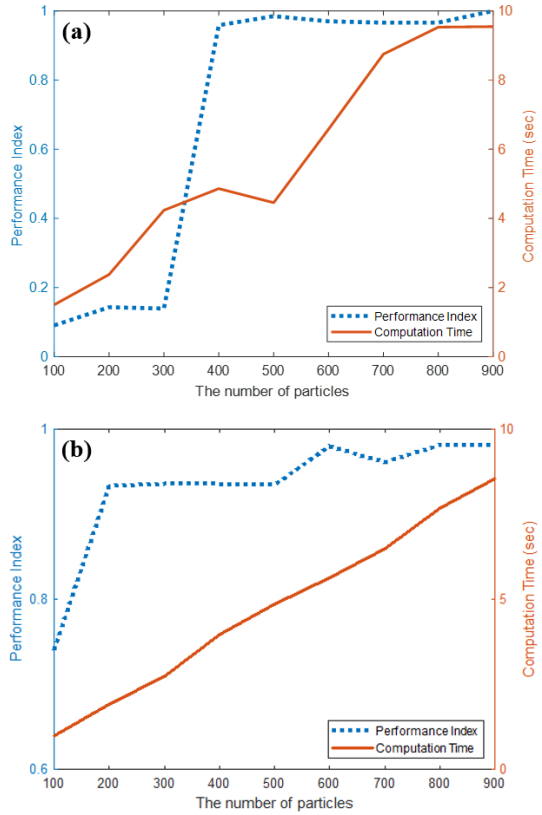

FIGURE 14. Performance indices and computation times according to the number of particles in the PSO. The performance index and the computation time increase as the number of particles increases. (a) The case of merging $\mathbf{M}_1$ and $\mathbf{M}_2$ (b) The case of merging $\mathbf{M}_2$ and $\mathbf{M}_3$.

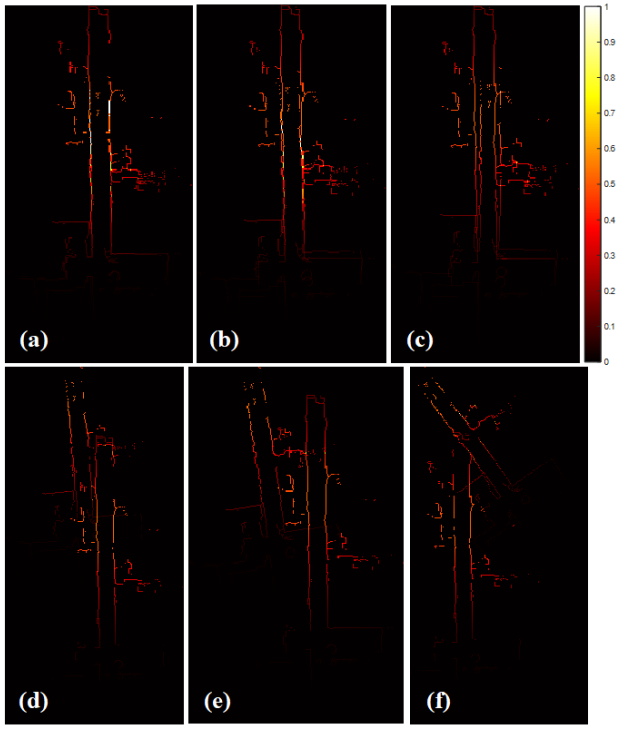

FIGURE 15. Map merging results of $\mathbf{M}_1$ and $\mathbf{M}_2$ with the proposed method and other methods. (a) Proposed. (b) SMM only (c) MSE (d) HCD (e) STCD (f) SURF.

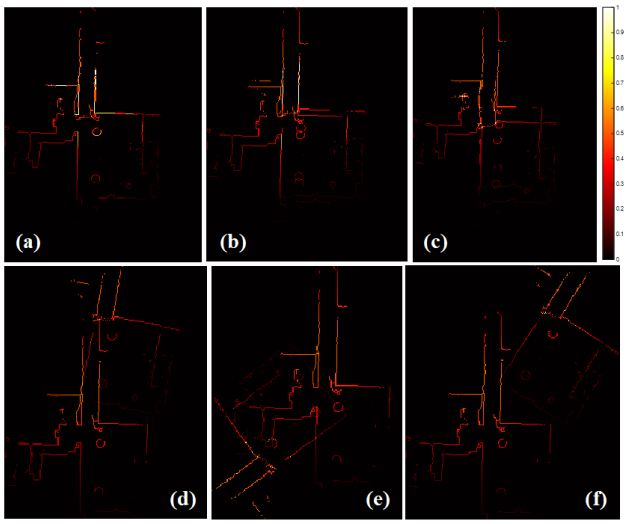

FIGURE 16. Map merging results of $\mathbf{M}_2$ and $\mathbf{M}_3$ with the proposed method and other methods. (a) Proposed. (b) SMM only (c) MSE (d) HCD (e) STCD (f) SURF.

calculation time according to the number of samples N_s were investigated, while I_a and Σ_a were fixed at 100 and 105, respectively. As shown in Fig. 14, the performance index and calculation time increase as the number of particles increases. All values in the figure were averaged over 10 trials. As a result, we found that the proper number of particles satisfying both the case of merging $\mathbf{M}_1$ and $\mathbf{M}_2$ and the case of merging $\mathbf{M}_2$ and $\mathbf{M}_3$ is more than 400. These results may be varying according to the quality and size of individual grid maps and the accuracy of unilateral observation measurements. A certain fact is that the more the number of particles, the better the accuracy of map merging. Therefore, if the robot system has sufficient processing power, it is recommended to use a sufficient number of particles for the accuracy of map merging.

C. COMPARISONS

To compare the accuracy of the proposed map merging method with other map merging methods, we applied the existing five map merging methods to merging the same individual maps. They were the method to use only the SMM, mean squared error (MSE) based image registration method, Harris corner detector (HCD) [20] based map matching, Shi-Tomasi corner detector (STCD) [21] based map matching, and speeded up robust features (SURF) [22] based map matching methods. The visual feature-based map merging methods such as MSE, HCD, STCD, and SURF were conducted as follows. First, the visual features were extracted from individual grid map images. Next, the RANSAC (Random sample consensus) algorithm was conducted to find the best map transformation while overcoming outliers in the

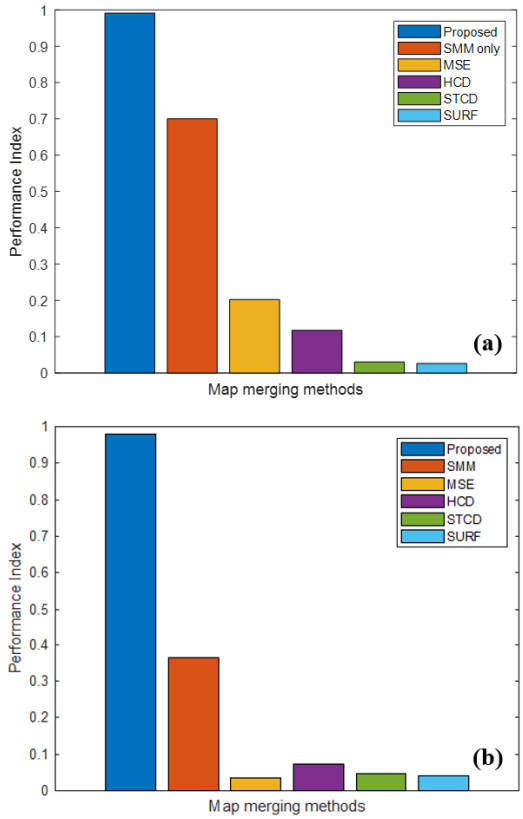

FIGURE 17. Comparison results with other map merging methods. The proposed method was more accurate than other map merging methods. (a) The case of merging M_1 and M_2 (b) The case of merging M_2 and M_3.

pairs of visual features. Finally, an individual grid map was transformed into the other individual grid map.

The graphical comparison of map merging results were shown in Fig. 15 and Fig. 16. The accuracy of map merging was quantitatively measured as the performance index defined in equation (14) after map merging. The comparison result is shown in Fig. 17. Obviously, the proposed map merging technique showed a higher performance index than other map merging techniques. However, even though the proposed method sometimes converges rapidly, the computation time was longer than other methods due to the iterative process of PSO. In future work, the proposed method will be accelerated using a field-programmable gate array (FPGA) based parallel computing method [23].

V. CONCLUSION

This paper proposed a unilateral observation-based map merging method for cooperative mapping in multi-robot systems. The proposed method can maintain the efficiency of multi-robot system operation by utilizing unilateral observation instead of unilateral observation. The risk of local minima in the conventional map matching method was avoided by unilateral observation-based map augmentation which can reduce the search space for relative poses among robots. To improve the accuracy of the MTM obtained by the unilateral observation-based map matching method, a sampling-based optimization method was applied and showed better accuracy. The proposed technique was tested by datasets acquired from real experiments using three mobile robots equipped with a sensor fusion system. The evaluation results showed that the proposed method works well with appropriate augmentation parameters and the enough number of particles. The comparison results showed that the proposed method can find a more accurate MTM than other methods.

REFERENCES

[1] H.-C. Lee and B.-H. Lee, "Improved feature map merging using virtual supporting lines for multi-robot systems," *Adv. Robot.*, vol. 25, nos. 13–14, pp. 1675–1696, Jan. 2011.

[2] H.-C. Lee, S.-H. Lee, M. H. Choi, and B.-H. Lee, "Probabilistic map merging for multi-robot RBPF-SLAM with unknown initial poses," *Robotica*, vol. 30, no. 2, pp. 205–220, Mar. 2012.

[3] H.-C. Lee and B.-H. Lee, "Enhanced-spectrum-based map merging for multi-robot systems," *Adv. Robot.*, vol. 27, no. 16, pp. 1285–1300, Nov. 2013.

[4] H. C. Lee, Y. J. Cho, and B. H. Lee, "Accurate map merging with virtual emphasis for multi-robot systems," *Electron. Lett.*, vol. 49, no. 15, pp. 932–934, Jul. 2013.

[5] H. C. Lee, B. S. Roh, and B. H. Lee, "Multi-hypothesis map merging with sinogram-based PSO for multi-robot systems," *Electron. Lett.*, vol. 52, no. 14, pp. 1213–1214, Jul. 2016.

[6] H. Lee, "Tomographic feature-based map merging for multi-robot systems," *Electronics*, vol. 9, no. 1, p. 107, Jan. 2020.

[7] H. Lee, "One-way observation-based cooperative robot mapping," in *Proc. IEEE 16th Int. Conf. Autom. Sci. Eng. (CASE)*, Aug. 2020, pp. 900–905.

[8] X. Zhou and S. Roumeliotis, "Multi-robot SLAM with unknown initial correspondence: The robot rendezvous case," in *Proc. IEEE/RSJ Int. Conf. Intell. Robots Syst.*, Oct. 2006, pp. 1785–1792.

[9] F. Tungadi, W. L. D. Lui, L. Kleeman, and R. Jarvis, "Robust online map merging system using laser scan matching and omnidirectional vision," in *Proc. IEEE/RSJ Int. Conf. Intell. Robots Syst.*, Oct. 2010, pp. 7–14.

[10] C. A. V. Hernandez and F. A. P. Ortiz, "A real-time map merging strategy for robust collaborative reconstruction of unknown environments," *Expert Syst. Appl.*, vol. 145, pp. 1–12, May 2020.

[11] M. Drwiega, "Features matching based merging of 3D maps in multi-robot systems," in *Proc. 24th Int. Conf. Methods Models Autom. Robot. (MMAR)*, Aug. 2019, pp. 663–668.

[12] Á. L. García, R. B. Navarro, L. M. B. Pascual, E. L. Guillén, M. O. Miguel, and D. S. Gómez, "SLAM and map merging," *J. Phys. Agents (JoPha)*, vol. 3, no. 1, pp. 13–23, 2009.

[13] K. Wang, S. Jia, Y. Li, X. Li, and B. Guo, "Research on map merging for multi-robotic system based on RTM," in *Proc. IEEE Int. Conf. Inf. Autom.*, Jun. 2012, pp. 156–161.

[14] S. Carpin, "Fast and accurate map merging for multi-robot systems," *Auto. Robots*, vol. 25, no. 3, pp. 305–316, Oct. 2008.

[15] L. A. F. Fernandes and M. M. Oliveira, "Real-time line detection through an improved Hough transform voting scheme," *Pattern Recognit.*, vol. 41, no. 1, pp. 299–314, Jan. 2008.

[16] J. Radon, "On the determination of functions from their integral values along certain manifolds," *IEEE Trans. Med. Imag.*, vol. MI-5, no. 4, pp. 170–176, Dec. 1986.

[17] S. Lee, H. Kim, and B. Lee, "An efficient rescue system with online multi-agent SLAM framework," *Sensors*, vol. 20, no. 1, p. 235, Dec. 2019.

[18] A. Doucet, A. Logothetis, and V. Krishnamurthy, "Stochastic sampling algorithms for state estimation of jump Markov linear systems," *IEEE Trans. Autom. Control*, vol. 45, no. 2, pp. 188–202, Feb. 2000.

[19] J. Kennedy and R. Eberhart, "Particle swarm optimization," *Proc. IEEE Int. Conf. Neural Netw.*, Nov. 1995, pp. 1942–1948.

[20] C. Harris and M. Stephens, "A combined corner and edge detector," in *Proc. Alvey Vis. Conf.*, 1988, pp. 147–151.

[21] J. Shi and Tomasi, "Good features to track," in *Proc. IEEE Conf. Comput. Vis. Pattern Recognit. (CVPR)*, Jun. 1994, pp. 593–600.
[22] H. Bay, A. Ess, T. Tuytelaars, and L. Van Gool, "SURF: Speeded up robust features," *Comput. Vis. Image Understand.*, vol. 110, no. 3, pp. 346–359, 2008.
[23] H. Lee, K. Kim, Y. Kwon, and E. Hong, "Real-time particle swarm optimization on FPGA for the optimal message-chain structure," *Electronics*, vol. 7, no. 11, p. 274, Oct. 2018.

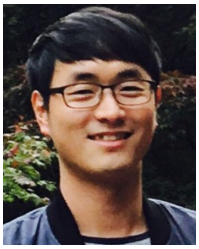

HEONCHEOL LEE (Member, IEEE) received the B.S. degree in electronic engineering and computer sciences from Kyungpook National University, Daegu, South Korea, in 2006, and the M.S. and Ph.D. degrees in electrical engineering and computer sciences from Seoul National University, Seoul, South Korea, in 2008 and 2013, respectively. From 2013 to 2019, he was a Senior Researcher with Agency for Defense Development, Daejeon, South Korea. Since 2019, he has been an Assistant Professor with the School of Electronic Engineering, Kumoh National Institute of Technology, Gumi, South Korea. He is a Technical Advisor with the Robot Navigation Division, Cleaning Science Research Institute, and LG Electronics. His research interests include SLAM, robot navigation, machine learning, real-time embedded systems, prognostics, and health management.

SEUNGHWAN LEE (Member, IEEE) received the B.S. degree in electronic engineering and computer sciences from Kyungpook National University, Daegu, South Korea, in 2008, and the M.S. and Ph.D. degrees in electrical engineering and computer sciences from Seoul National University, Seoul, South Korea, in 2010 and 2015, respectively. From 2015 to 2018, he was a Senior Researcher with the Samsung Electronics Mechatronics and Manufacturing Technology Center, Suwon, South Korea. Since 2018, he has been an Assistant Professor with the School of Electronic Engineering, Kumoh National Institute of Technology, Gumi, South Korea. His research interests include multi-robot SLAM and coverage path planning.